



Enhancing activity in a nanostructured BiVO₄ photoanode with a coating of microporous Al₂O₃



Murilo F. Gromboni^a, Dyovani Coelho^a, Lucia H. Mascaro^{a,*}, Adam Pockett^b, Frank Marken^{b,*}

^a Department of Chemistry, Federal University of São Carlos, Rod. Washington Luiz, Km 235, CEP 13565-905, São Carlos, SP, Brazil

^b Department of Chemistry, University of Bath, Claverton Down, Bath, BA2 7AY, UK

ARTICLE INFO

Article history:

Received 30 April 2016

Received in revised form 17 June 2016

Accepted 23 June 2016

Available online 24 June 2016

Keywords:

Water splitting

Solar energy

Photocatalysis

Ceramic coating

Photo-kinetics

Microporous membrane

ABSTRACT

Nanostructured semiconductor photoanodes play an important role in solar fuel generation, and the design of the semiconductor – aqueous electrolyte interface can be crucial in enhancing the energy conversion efficiency. We have investigated the effects on photoelectrochemical oxygen evolution for monoclinic nanostructured BiVO₄ films uncoated and coated with microporous sol-gel Al₂O₃ “over-layers”. Variation of the thickness of the Al₂O₃ coating (formed by surface sol-gel deposition and annealing at 435 °C) led to a reduction of pseudo-capacitance and allowed optimization of the quantum efficiency. Exploration of the photocurrent enhancement as a function of applied potential reveals two distinct potential domains/mechanisms: (i) a low bias region enhancement effect (assigned to a lowering of the rate of external recombination of electrons with oxygen) and (ii) a high bias region of enhancement (assigned to higher charge carrier mobility due to less trapping in surface states).

© 2016 Elsevier B.V. All rights reserved.

1. Introduction

Photochemical reactivity at semiconductor-aqueous solution interfaces is determined by many factors including (i) charge carrier transport to the semiconductor|water interface and partitioning/trapping in the “interfacial reaction zone”, (ii) the nature/mobility of reactive surface species taking part in photocatalytic processes, and (iii) the dielectric conditions and double layer structure at the interface [1]. The processes taken place in semiconductor nano-structures during photoelectrochemical reactions (for example in solar water splitting [2]) are complex and depend on multiple parameters since they may involve multiple mechanistic pathways, that include multiple (internal and external) recombination and loss mechanisms. An attractive tool for the enhancement of photo-catalytic reactivity, for example for solar water splitting, is the formation of “over-layers” or “blocking-layers”. For hematite, Fe₂O₃, it was observed that photo-electrochemical performance can be improved by coating the oxide with very thin Al₂O₃ over-layers [3]. The role of Al₂O₃ in these processes may at least in part be chemical and in part electronic and attributed to changes in surface conditions for the underlying semiconductor [4], which experi-

ences a “coating medium” with a dielectric constant lower than that of the aqueous electrolyte ($\epsilon_{\text{water}} = 80.2$ at 20 °C [5]; $\epsilon_{\text{Al}_2\text{O}_3} = 9.34$ at 25 °C [6]). The coating could also passivate surface states or change/restrict access for ionic solution species. As a result, the ability of holes/electrons to be trapped into surface states would be altered and correspondingly their apparent mobility/reactivity altered.

In addition to exerting electronic effects and changes in charge carrier transport, “over-layers” can also have beneficial effects on the transport of reactive solution species to the electrode surface. Barrier coatings at semiconductor – electrolyte interfaces can be crucial for the effective operation of solar electrolyser devices. The effect of a hydrogen permeable Cr₂O₃ [7] in suppressing recombination via back-reaction with oxygen in water splitting processes is a good example. Access of oxygen to the Rh or Pt metal catalyst coated with Cr₂O₃ is avoided and therefore recombination (here as back-reaction with oxygen) can be suppressed. Similarly, for Al₂O₃ deposits on semiconductors, a blocking effect on oxygen reaching the semiconductor photoanode surface or the underlying substrate would be beneficial for stopping losses due to back reaction via electron transfer to oxygen.

Initial studies on the sol-gel Al₂O₃ deposition process were reported by Ichinose et al. [8], and experimental methods were developed for thin layer “surface-sol-gel” formation [9]. Kumara et al. [10] reported enhanced photocurrents from SnO₂

* Corresponding authors.

E-mail address: f.marken@bath.ac.uk (F. Marken).

photo-anodes in dye-sensitized solar cells when coated with Al_2O_3 . In this case, a sensitiser dye was immobilized directly onto the surface of the Al_2O_3 film. $\text{TiO}_2\text{--SnO}_2$ composite electrodes were shown to perform better with Al_2O_3 barrier coatings [11]. The application of microporous Al_2O_3 as a photo-current enhancing coating in photo-electrochemical systems is now relatively common. Durrant et al. [12] further developed these coatings based on the surface-sol-gel deposition recipe for Al_2O_3 on TiO_2 film electrodes [13]. These were then employed to host sensitizer dye in a dye-sensitized solar cell [14] and found to considerably increase performance. More recently, also atomic layer deposition (ALD) methods have been suggested for Al_2O_3 barrier layer coatings [15–17]. Effects primarily on electron tunnel kinetics based on the more dense and less/non-porous ALD Al_2O_3 films have been discussed [18]. Aligned TiO_2 nanotube arrays were studied and exhibited ALD Al_2O_3 coating thickness dependent efficiency as dye-sensitized solar cells [19]. ALD coating offers a powerful surface modification tool for dense conformal coatings. However, most literature studies to date have been based on microporous surface-sol-gel Al_2O_3 over-layers.

A flexible solar cell device based on mesoporous TiO_2 coated with Al_2O_3 and immobilized ruthenium dye was reported [20], for which the microporous Al_2O_3 film was an integral component stopping short circuit reactions and enhancing photo-activity. A novel photovoltaic “charge storing” hetero-junction device was obtained by Kim et al. while investigating $\text{TiO}_2\text{--Al}_2\text{O}_3\text{--WO}_3$ materials in aqueous electrolyte [21]. Effects were assigned to an improved charge trapping for electrons in WO_3 and less recombination across the Al_2O_3 film. Generally, there seems to be agreement in the liter-

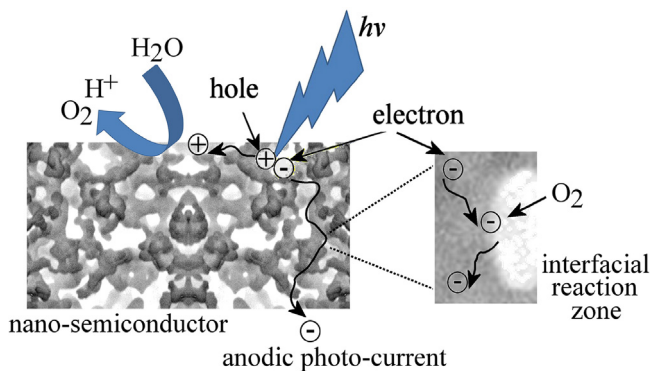


Fig. 1. Schematic drawing of the photo-anode mechanism for a nano-structured semiconductor fully “shielded” in aqueous electrolyte solution. In this electrolyte shielded nano-structure hole-electron pairs are generated and split into surface confined holes (resulting in oxygen evolution) and mobile electrons (diffusing through the nano-structure). Both recombination (internal and external back reaction with oxygen) and electron mobility (dependent on trap states) are affected by the interfacial reaction zone (e.g. the presence of Al_2O_3 coatings).

ature that it is predominantly recombination rates (via external back-reactions) that are affected when thin Al_2O_3 coatings are applied [22]. Beneficial effects of microporous Al_2O_3 have also been observed on NiO photo-cathodes where hydrogen evolution is the predominant process [23] and on CdSe sensitized NiO [24]. Single molecule studies for charge injection from excited dye into NiO via Al_2O_3 suggest a slowing down in electron transfer kinetics [25].

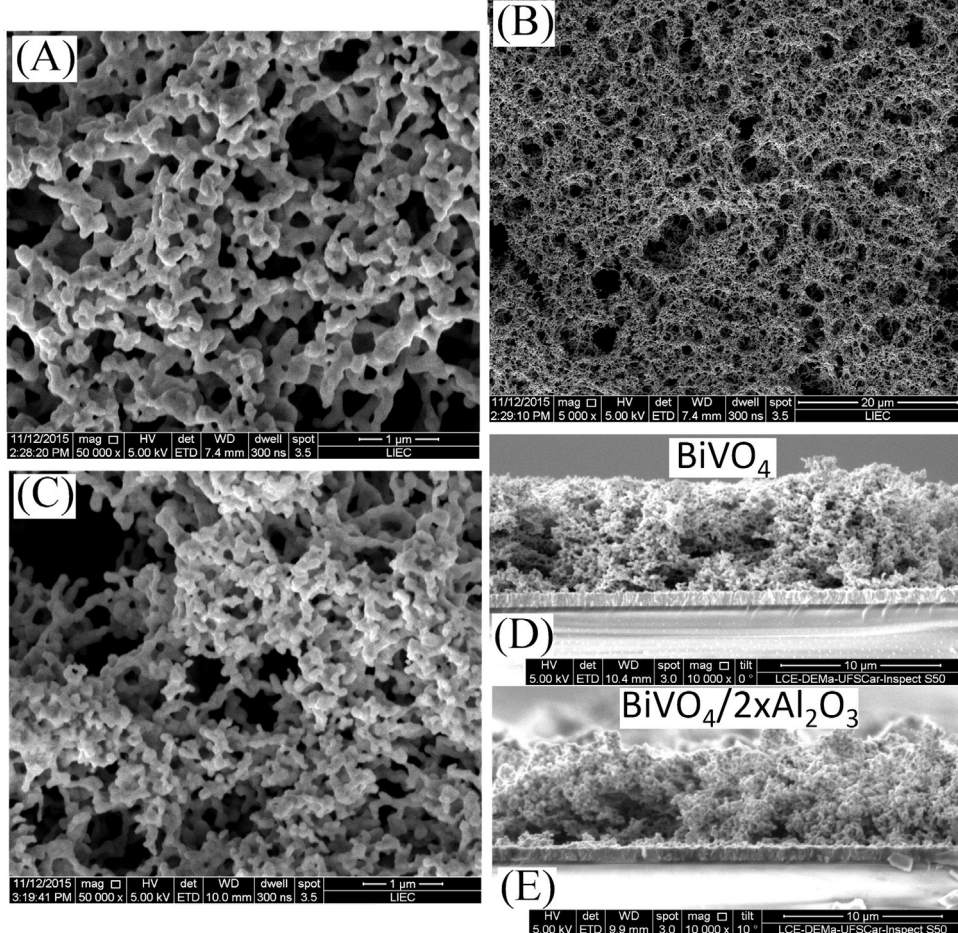


Fig. 2. (A,B) FE-SEM images of “one-step” BiVO_4 films obtained with $10 \mu\text{L cm}^{-2}$ “paint” dropped and annealed on FTO at 400°C . (C) FE-SEM image of a $\text{BiVO}_4/2\text{Al}_2\text{O}_3$ film deposit. (D,E) Cross-sectional FE-SEM images for BiVO_4 and $\text{BiVO}_4/2\text{Al}_2\text{O}_3$, respectively.

Beneficial effects of Al_2O_3 coatings on ZnO -based dye-sensitized solar cells were investigated as a function of thickness [26]. Solution processed Al_2O_3 were also employed in organic photovoltaic devices [27] and hybrid devices [28]. In photocatalysis, TiO_2 films were coated with $\text{Al}_2\text{O}_3/\text{Pt}$ to improve hydrogen evolution and efficiency in dechlorination reactions [29].

BiVO_4 [30,31] and in particular nano-structured BiVO_4 [32–34], are attractive photo-anode materials for photo-catalysis and water splitting applications, but the effect of Al_2O_3 over-layers has not been reported previously. We have recently reported a simple “one-step” approach for the formation of BiVO_4 from a paint precursor applied to tin-doped indium oxide (ITO) substrates [35] and for application of BiVO_4 coatings onto titanium substrates [36]. The resulting monoclinic BiVO_4 has a bright yellow colour and therefore offers an effective absorption band in the visible range of the optical spectrum (with a band gap of typically 2.5 eV). Photocurrents have been optimized to reach 2.4 mA cm^{-2} at 1.23 V vs. RHE and under one sun (AM1.5 or ca. 100 mW cm^{-2}) illumination [37]. Materials engineering approaches have been reported to further improve performance based on inclusion of phosphate [38], lanthanum [39], iridium [40], molybdenum [41], cobalt [42], nickel [43], TiO_2 [44–46], and WO_3 [47]. The geometry of Mo-doped BiVO_4

was further optimized in macro-microporous “inverse opal” structures [48].

In this report, microporous surface-sol-gel Al_2O_3 is applied to nanostructured BiVO_4 photo-anodes. The morphology features of this BiVO_4 semiconductor nanostructure are relatively small (typically 100 nm in diameter) and surrounded by aqueous electrolyte to provide “electrolyte shielded” conditions with electron diffusion towards the substrate [49] (in contrast to conditions at a flat single crystal semiconductor surface). The Al_2O_3 film is produced based on Durrant’s sol-gel procedure [12] to give very thin microporous film coatings with only a few nanometer thickness. A schematic drawing of the resulting interface with interfacial reaction zone (e.g. for $\text{BiVO}_4 | \text{Al}_2\text{O}_3 | \text{electrolyte}$) is shown in Fig. 1. Two distinct recombination pathways are possible: (i) internal (direct hole-electron recombination) and (ii) external (back-reaction of electrons in surface states with oxygen in solution). The mobility of electrons could be affected by the availability/absence of “trap states” at the semiconductor surface. Therefore, both recombination and electron transport can play an important role in determining the magnitude of the photocurrent. The enhancing effect of the microporous Al_2O_3 over-layer is studied as a function of thickness (or the number of applied coatings) and shown to be effective in

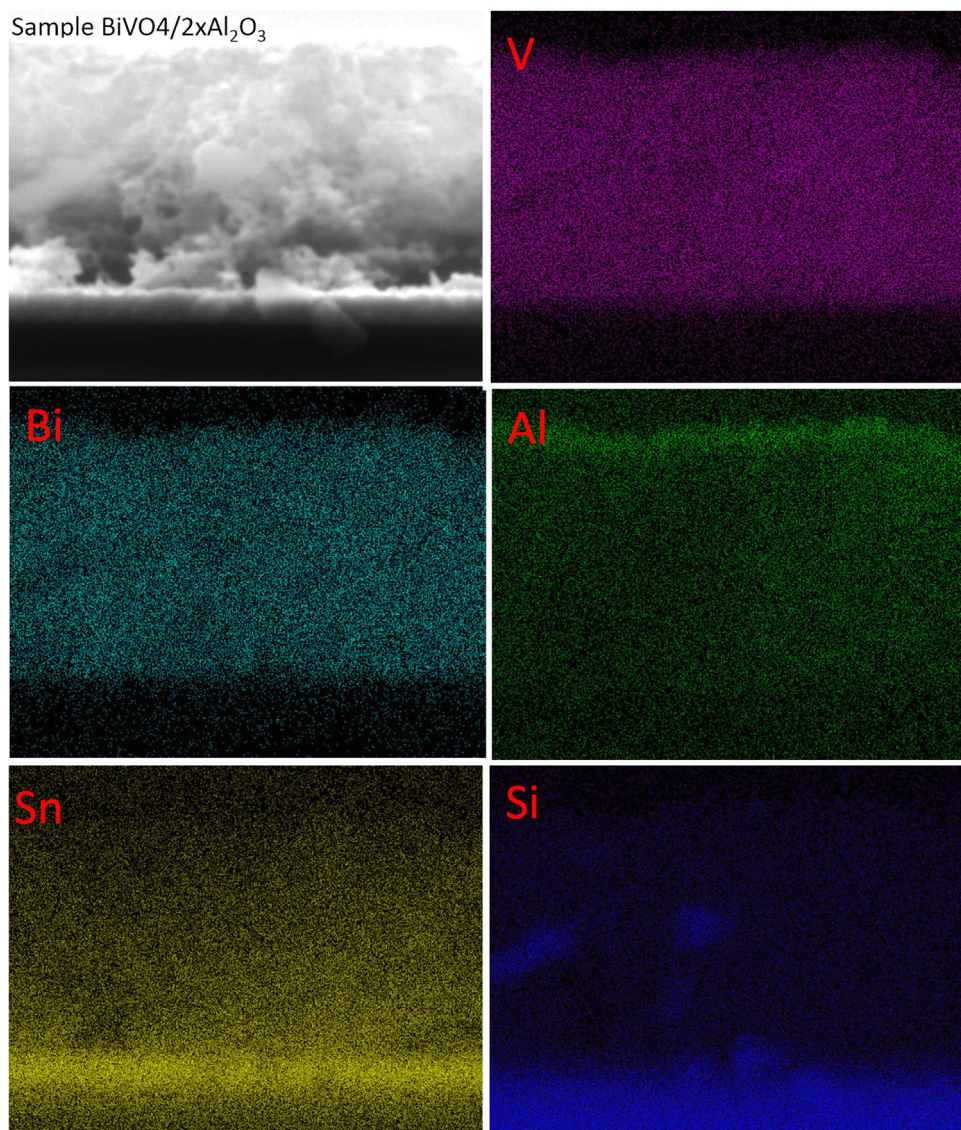


Fig. 3. Cross-sectional FE-SEM with elemental mapping (V, Bi, Al, Sn, Si) for a $\text{BiVO}_4/2\text{xAl}_2\text{O}_3$ film deposit on FTO.

particular at lower potential bias (possibly providing protection against external recombination via back-reaction) and at higher potential bias (possibly providing faster charge carrier transport and protection against internal recombination). The important role of the available surface redox states (which are linked to interfacial pseudo-capacitance) in the process is analyzed.

2. Experimental section

Chemical reagents were $\text{Bi}(\text{NO}_3)_3 \cdot 5\text{H}_2\text{O}$, NH_4VO_3 , $\text{Al}[\text{OCH}(\text{CH}_3)\text{C}_2\text{H}_5]_3$ (in dichloromethane), ethylene glycol, and PEG300 (all Sigma-Aldrich). The supporting electrolyte for photo-voltammetric measurements was aqueous 0.5 mol dm^{-3} di-sodium sulphate. All chemicals were of analytical grade. Ultra-pure water ($18.2\text{ M}\Omega\text{ cm}$) was taken from a Milli-Q Simplicity 185 system (Millipore).

The photo-electrodes were prepared following a slightly modified literature procedure based on the previously published one-step approach [35]. Precursor solutions for BiVO_4 films were prepared by mixing (A) a suspension with 0.2 mol dm^{-3} NH_4VO_3 in $2\text{ mL H}_2\text{O}$ at 80°C and (B) a solution of 0.4 mol dm^{-3} $\text{Bi}(\text{NO}_3)_3$ in 1 mL PEG300 :ethylene glycol (1:1). After 30 min sonication a uniform paint was obtained. For coating of the FTO substrates, first the substrates were heated to 85°C and an aliquot paint of typically $10\text{ }\mu\text{L cm}^{-2}$ of prepared paint was applied. The samples were then dried for 10 min at 120°C . Next, samples were calcined in air for 60 min at 400°C . After calcination, the oven was turned off and the samples cooled to ambient conditions. The Al_2O_3 overcoating process was performed following a slightly modified literature procedure based on the methodology developed by Durant and coworkers [50]. The BiVO_4 electrode was coated with a microporous aluminium oxide overlayer by dropping $10\text{ }\mu\text{L cm}^{-2}$ from an aliquot of 0.15 M solution of aluminium tri-sec-butoxide in 2-propanol/dichloromethane. The electrode was then nitrogen-flow-dried and annealed in a tube furnace at 435°C for 20 min. The procedure was repeated for each layer of Al_2O_3 deposited.

The photo-electrochemical measurements were performed with a potentiostat/galvanostat (Autolab PGSTAT 302N, Metrohm-Eco Chemie) using GPES and FRA 4.9 software. The light source was a blue power LED with $\lambda = 455\text{ nm}$ (Thorlabs, UK). A three-electrode conventional electrochemical cell with quartz windows was used. The reference electrode was Ag/AgCl in 3 M KCl (BAS), the auxiliary electrode was a platinum plate, and working electrodes were BiVO_4/FTO photo-anodes. The light input through the quartz window of the electrochemical cell was estimated as ca. 100 mW cm^{-2} (employing a semiconductor photodiode, Thorlabs) with optical path of ca. 0.5 cm from quartz window to electrode surface. Cyclic voltammetry (CV) experiments were carried out in 0.5 mol L^{-1} Na_2SO_4 ($\text{pH} = 5.3$) as supporting electrolyte and the photo-electrodes were illuminated from the front or back side. The crystalline phase of nano- BiVO_4 and $\text{BiVO}_4/\text{Al}_2\text{O}_3$ was characterized by X-ray diffraction (XRD) using a Shimadzu diffractometer model XRD-6000, in θ - 2θ mode, from 10 to 80° , rate 2° s^{-1} , and accelerating voltage 30 kV . The morphology and thickness of the film were evaluated by high-resolution field emission scanning electron microscopy (FE-SEM, Zeiss Supra 35 at 2 kV).

3. Results and discussion

3.1. Deposition and characterisation of BiVO_4 and $\text{BiVO}_4/\text{Al}_2\text{O}_3$ films on fluorine-doped tin oxide (FTO)

Deposition of BiVO_4 from a “paint” precursor onto fluorine-doped tin oxide (FTO) transparent conducting film electrodes was performed following a recipe reported recently [35]. Here, this

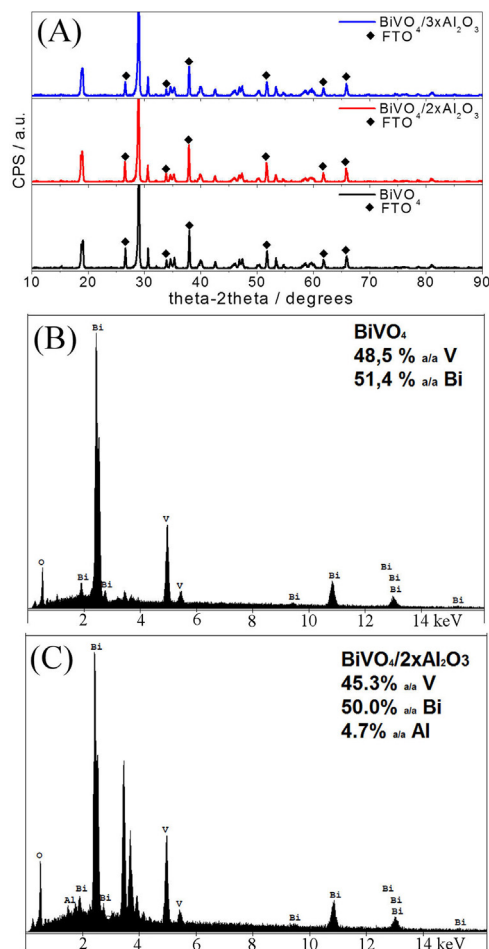


Fig. 4. (A) XRD data for BiVO_4 , $\text{BiVO}_4/2\text{Al}_2\text{O}_3$, and $\text{BiVO}_4/3\text{Al}_2\text{O}_3$ film deposits showing FTO substrate diffraction peaks as well as monoclinic BiVO_4 (consistent with PDF: 01-083-1699) and (B) EDS spectra for $\text{BiVO}_4/2\text{Al}_2\text{O}_3$.

methodology was modified by annealing at a milder temperature of 400°C . Scanning electron micrographs (SEMs) are shown in Fig. 2A and B. In contrast to material produced at 500°C [35] with feature sizes of typically $1\text{ }\mu\text{m}$, here with an annealing temperature of 400°C the feature size of the nano-structured BiVO_4 deposit is typically $0.1\text{ }\mu\text{m}$ or an order of magnitude smaller due to less structural annealing at lower temperature. The thickness of films is typically ca. $7\text{--}8\text{ }\mu\text{m}$ (see Fig. 2D). With the surface-sol-gel Al_2O_3 coating applied, there is only insignificant change in electron optical images (see Fig. 2C and D), which suggests that only very thin and very uniform Al_2O_3 coatings are formed.

Additional cross-section elemental mapping was performed for a sample of BiVO_4 with 2 layers of Al_2O_3 applied to the surface (Fig. 3). The presence of both Bi and V uniformly distributed throughout the film is observed. Perhaps surprisingly, there is some Sn (originating from the substrate) distributed throughout the film. Traces of Si are likely to be due to the sample preparation/cutting process. The distribution of Al shows some excess at the top surface (a layer of ca. $1\text{ }\mu\text{m}$ thickness) with further Al being found throughout the nanostructured film. The XRD pattern for the BiVO_4 film (Fig. 4A) is consistent with the monoclinic phase [30]. Additional XRD peaks for Al_2O_3 are not observed when BiVO_4 films are modified with 2 or 3 layers of Al_2O_3 , presumably due to the very thin coating and small grain size developed for the microporous sol-gel Al_2O_3 . However, the signature for Al is clearly detected from EDS analysis, where Al content was 4.7% at/at (Fig. 4C).

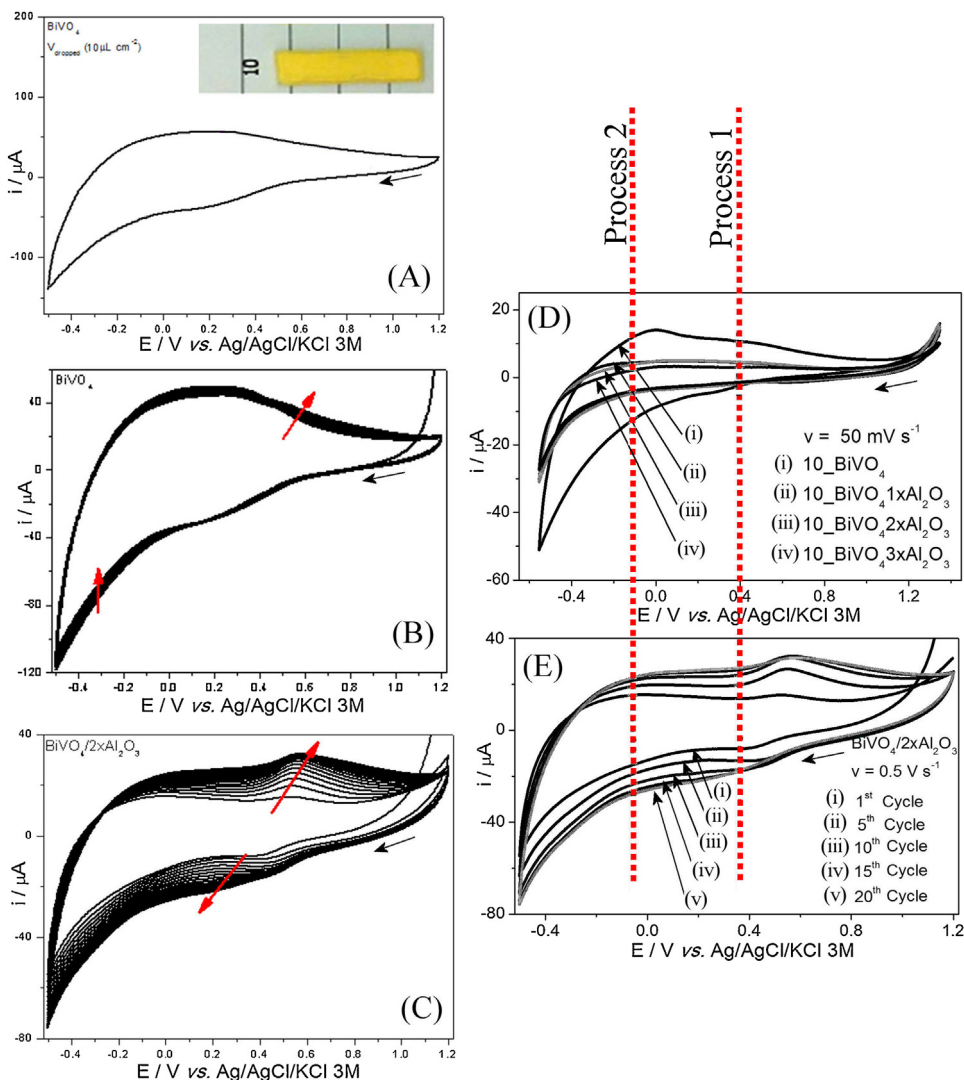
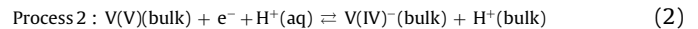
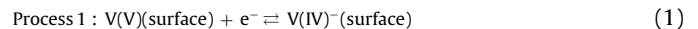


Fig. 5. (A) Cyclic voltammogram ($0.5 \text{ mol dm}^{-3} \text{ Na}_2\text{SO}_4$, 20th potential cycle shown; scan rate 500 mV s^{-1}) for a “one-step” BiVO_4 film electrode produced at 400°C (Inset: photograph). (B) Cyclic voltammograms for BiVO_4 in $0.5 \text{ mol dm}^{-3} \text{ Na}_2\text{SO}_4$ at scan rate 500 mV s^{-1} (twenty potential cycles shown). (C) As above, but for $\text{BiVO}_4/2\text{Al}_2\text{O}_3$. (D) Cyclic voltammogram for samples BiVO_4 , $\text{BiVO}_4/1\text{Al}_2\text{O}_3$, $\text{BiVO}_4/2\text{Al}_2\text{O}_3$, $\text{BiVO}_4/3\text{Al}_2\text{O}_3$ in $0.5 \text{ mol dm}^{-3} \text{ Na}_2\text{SO}_4$, twenty-first potential cycle shown; scan rate 50 mV s^{-1} . (E) The 1st, 5th, 10th, and 20th potential cycle for $\text{BiVO}_4/2\text{Al}_2\text{O}_3$ shown at scan rate 500 mV s^{-1} .

The optical appearance of films after annealing is yellow and non-transparent (see photograph in Fig. 5A) with a film thickness estimated as ca. $7\text{--}8 \mu\text{m}$ for $10 \mu\text{L cm}^{-2}$ “paint” precursor. Film formation and photocurrents (with back illumination, *vide infra*) are highly reproducible, presumably due to the considerable thickness of these non-transparent films (which minimizes effects from film thickness variations). Based on literature reports, even Al_2O_3 layers of less than 1 nm average thickness can result in significant photocurrent enhancement [51]. The coating is therefore unlikely to be directly detectable in SEM and likely to be applied throughout the structure (see EDS mapping in Fig. 3) as well as onto the underlying FTO substrate electrode.

In “dark” electrochemical experiments (see Fig. 5) in aqueous $0.5 \text{ M} \text{ Na}_2\text{SO}_4$ the presence of the BiVO_4 is clearly detected as a reduction signal with onset at approximately 0.6 V vs. Ag/AgCl ($3 \text{ M} \text{ KCl}$). At a slightly faster scan rate (see Fig. 5D) two distinct and chemically reversible redox processes are observed centered at 0.35 V vs. Ag/AgCl ($3 \text{ M} \text{ KCl}$) (Process 1) and at -0.06 V vs. Ag/AgCl ($3 \text{ M} \text{ KCl}$) (Process 2). The former is likely to be associated with V(V/IV) surface redox chemistry (Eq. (1)) and the latter with bulk

V(V/IV) conversion associated with cation intercalation [35] (Eq. (2)).



With sol-gel Al_2O_3 applied to the electrode surface, both processes 1 and 2 are suppressed (see Fig. 5C) and with repeated potential cycling process 1 can be seen to slowly re-emerge to some extent (now shifted positive by 0.15 V to a potential of 0.50 V vs. Ag/AgCl ($3 \text{ M} \text{ KCl}$), see Fig. 5E). This behavior could be associated with some leaching of vanadate through/onto the micro-porous Al_2O_3 film deposit. This “ageing” effect is not observed in photo-electrochemical experiments (*vide infra*). Importantly, both types of vanadium surface trap states (which are able to bind electrons, but which could also be involved in hole trapping) appear to be suppressed, which should have two beneficial effects on photoelectrochemical processes: (i) the transport of electrons through the nano- BiVO_4 network is facilitated (faster) with less trap states and (ii) the back-reaction with oxygen in the aqueous phase (recombination) at trap states is suppressed. Both of these effects should improve photoelectrochemical performance. In addition, the interfacial capacitance (or availability of surface

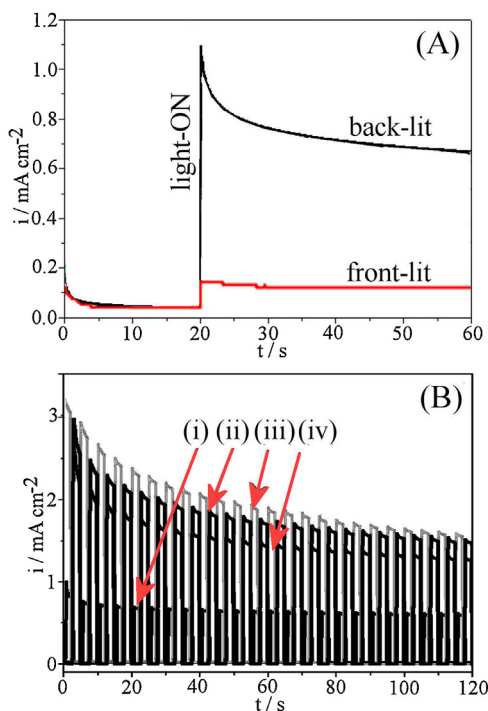


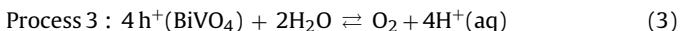
Fig. 6. (A) Light-on photocurrent transients (blue-LED light with 100 mW cm^{-2} , $\lambda = 455 \text{ nm}$) in $0.5 \text{ mol dm}^{-3} \text{Na}_2\text{SO}_4$ and $E_{\text{BIAS}} = +1.3 \text{ V}$ vs. Ag/AgCl (3 M KCl) under front-side and back-side illumination for $10 \mu\text{L cm}^{-2}$ BiVO_4 “paint” annealed at 400°C . (B) Photocurrent transients with $E_{\text{BIAS}} = +1.2 \text{ V}$ vs. Ag/AgCl (3 M KCl) comparing (i) 0, (ii) 1, (iii) 2, and (iv) 3 Al_2O_3 layers.

redox states) for $\text{BiVO}_4/2\text{Al}_2\text{O}_3$ can be seen to be lower (compared to BiVO_4) by a factor three approximately.

3.2. Photo-voltammetric characterisation of BiVO_4 and $\text{BiVO}_4/\text{Al}_2\text{O}_3$ films on fluorine-doped tin oxide (FTO)

Photocurrent transients of typically 1 mA cm^{-2} (at 1.3 V vs. Ag/AgCl (3 M KCl) applied potential) are observed for BiVO_4 coated FTO electrodes immersed in $0.5 \text{ M} \text{Na}_2\text{SO}_4$ (illuminated with a blue LED delivering approximately 100 mW cm^{-2} , see Fig. 6). By comparing front side illumination and back side illumination, a dramatic difference due to the thicker (non-transparent) nature of the BiVO_4 film can be observed (see Fig. 6A inset). For front illumination under otherwise identical conditions, only 10% of the photo-current magnitude is detected (due to light absorption predominantly in the region more distant from the electrode [52]).

The underlying redox process for the light-driven reaction has been identified as the formation of oxygen from water due to hole reactivity at the surface of BiVO_4 (Eq. (3)) [53]. The more mobile electrons find their way through the BiVO_4 nanostructure to the underlying substrate electrode to provide the anodic photocurrent response. It is the loss of these electrons in transit (see Eq. (1)) that explains the difference between back- and front-illumination.



When investigating the effect of sol-gel Al_2O_3 on the photoelectrochemical behavior (Fig. 6B), a clear increase in photocurrent at 1.2 V vs. Ag/AgCl (3 M KCl) is seen when going from zero to one and to two coatings. A third coating only has a small effect or in some cases even slightly decreases the photo-current response (Fig. 6B). Further coatings significantly decrease the photo-current responses.

When investigating the magnitude of the photocurrent enhancement as a function of the applied potential (Fig. 7) an interesting pattern emerges. The photocurrent enhancement is large (Fig. 7E) in particular at lower bias potentials. The current more

than doubles, which is indicative of suppression of recombination at low driving voltages. This is likely to be due to a lower rate of external recombination (blocked by Al_2O_3) based on oxygen back-reacting with electrons in surface states (see Figs. 1 and 7E). A further region of strong enhancement is at more positive potentials beyond 1.0 V vs. Ag/AgCl (3 M KCl) bias. In this potential range electrons are quickly removed into the underlying FTO substrate electrode. However, under these conditions, the microporous Al_2O_3 film is proposed to help harvesting electrons from deeper within the porous BiVO_4 film due to higher mobility (enhanced conductivity for electrons and less trapping in surface states). A summary of the two effects, at low bias and at higher bias is shown schematically in Fig. 7E. Effects of Al_2O_3 such as lowering recombination rates and enhancing charge carrier mobility have been suggested and reviewed recently for barrier coatings on other types of semiconductors [54].

4. Conclusions

It has been shown that thin microporous sol-gel Al_2O_3 coatings on BiVO_4 have a beneficial effect on photocurrents for oxygen evolution, in particular in the low potential bias and high potential bias domains. It is suggested here that the microporous Al_2O_3 at the semiconductor – aqueous electrolyte interface is effective due to (i) a lowering of the availability of surface redox states (trap states) which are reactive towards solution oxygen (leading to less external recombination at low bias) and (ii) a speeding up electron transport through the nano- BiVO_4 structure (leading to improved electron harvesting at high bias). Additional structural information showing how the Al_2O_3 film is distributed and orientated with respect to the underlying semiconductor would be desirable and more work will be necessary also to quantify rate constants and mechanistic pathways.

In this preliminary study only the photo-active BiVO_4 material produced at 400°C was investigated to provide proof-of-principle for improved photo-currents. The methodology will be of broader

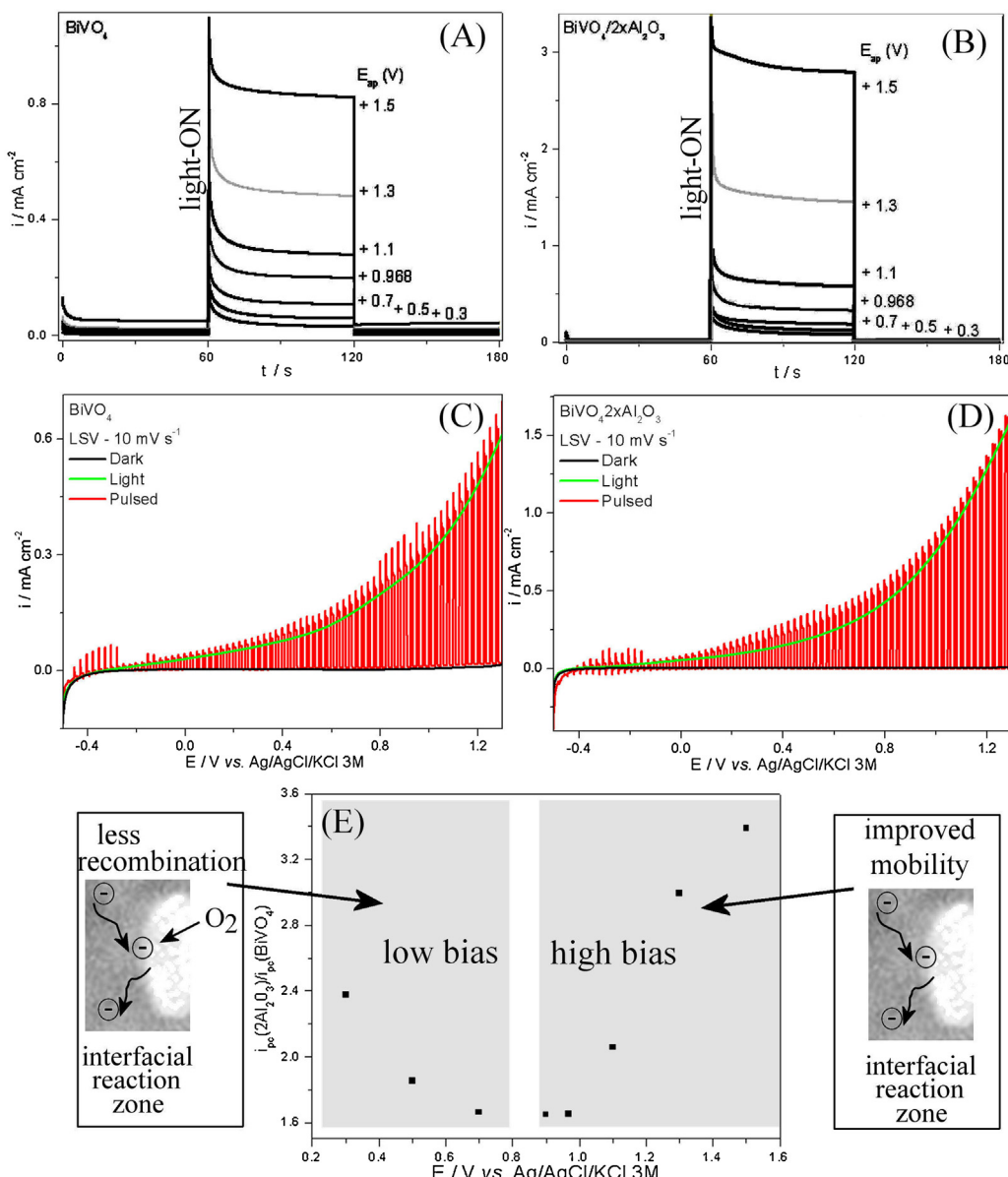


Fig. 7. Photocurrent transients for (A) BiVO_4 and (B) $\text{BiVO}_4/2\text{Al}_2\text{O}_3$ generated with a blue LED (100 mW cm^{-2} , $\lambda = 455 \text{ nm}$, 0.30 Hz , chronoamperometry at different E_{bias}) in $0.5 \text{ M Na}_2\text{SO}_4$ ($\text{pH} = 5.1$). Photocurrent transients for (C) BiVO_4 and (D) $\text{BiVO}_4/2\text{Al}_2\text{O}_3$ as a function of potential (linear sweep voltammetry, scan rate 10 mV s^{-1}). (E) The ratio of photocurrents detected for $\text{BiVO}_4/2\text{Al}_2\text{O}_3$ divided by that for BiVO_4 plotted versus bias potential and indicating two distinct potential regions.

appeal and useful also for related doped photo-catalyst materials. In addition to applications in solar fuel production, there could be interesting applications in selective photo-catalysis for processes exploiting solar electrosynthesis. Finally, in future the electrically insulating nature of Al_2O_3 will allow very thin wet “sandwich cells” to be constructed for solar energy harvesting with only oxygen redox mediation and a platinized counter electrode.

Acknowledgements

M.F.G. and L.H.M. and F.M. thank CAPES (PVE 71/2013) 327 and FAPESP (2013/07296-2) and CNPq (472384/2012-0) for financial support. We thank Professor Laurie M. Peter for discussion and support.

References

- [1] R. Memming, *Semiconductor Electrochemistry*, Wiley-VCH, Weinheim, 2015.
- [2] F.E. Osterloh, *Chem. Soc. Rev.* 42 (2013) 2294–2320.
- [3] F. Le Formal, N. Tetreault, M. Cornuz, T. Moehl, M. Grätzel, K. Sivula, *Chem. Sci.* 2 (2011) 737–743.
- [4] O. Neufeld, N. Yatom, M.C. Toroker, *ACS Catal.* 5 (2015) 7237–7243.
- [5] W.M. Haynes (Ed.), *CRC Handbook of Chemistry and Physics*, 95rd ed., CRC Press, 2014.
- [6] G.A. Parks, *Chem. Rev.* 65 (1965) 177–198.
- [7] K. Maeda, K. Teramura, D.L. Lu, N. Saito, Y. Inoue, K. Domen, *J. Phys. Chem. C* 111 (2007) 7554–7560.
- [8] I. Ichinose, H. Senzu, T. Kunitake, *Chem. Lett.* 10 (1996) 831–832.
- [9] I. Ichinose, H. Senzu, T. Kunitake, *Chem. Mater.* 9 (1997) 1296–1297.
- [10] G.R.R.A. Kumara, K. Tennakone, V.P.S. Perera, A. Konno, S. Kaneko, M. Okuya, *J. Phys. D: Appl. Phys.* 34 (2001) 868–873.
- [11] Z.Y. Liu, K. Pan, M. Liu, M.J. Wang, Q. Lu, J.H. Li, Y.B. Bai, T.J. Li, *Electrochim. Acta* 50 (2005) 2583–2589.
- [12] E. Palomares, J.N. Clifford, S.A. Haque, T. Lutz, J.R. Durrant, *Chem. Commun.* (2002).
- [13] E. Palomares, J.N. Clifford, S.A. Haque, T. Lutz, J.R. Durrant, *J. Am. Chem. Soc.* 125 (2003) 475–482.
- [14] B.C. O'Regan, S. Scully, A.C. Mayer, E. Palomares, J. Durrant, *J. Phys. Chem. B* 109 (2005) 4616–4623.
- [15] V. Ganapathy, B. Karunagaran, S.W. Rhee, *J. Power Sources* 195 (2010) 5138–5143.

- [16] A.F. Palmstrom, P.K. Santra, S.F. Bent, *Nanoscale* 7 (2015) 12266–12283.
- [17] W. Dong, T. Meng, Q. Chen, *Sci. Adv. Mater.* 7 (2015) 120–126.
- [18] C. Prasitichai, J.R. Avila, O.K. Farha, J.T. Hupp, *J. Am. Chem. Soc.* 135 (2013) 16328–16331.
- [19] J.Y. Kim, K.H. Lee, J. Shin, S.H. Park, J.S. Kang, K.S. Han, M.M. Sung, N. Pinna, Y.E. Sung, *Nanotechnology* 25 (2014) 504003.
- [20] S.A. Haque, E. Palomares, H.M. Upadhyaya, L. Otley, R.J. Potter, A.B. Holmes, J.R. Durrant, *Chem. Commun.* (2003) 3008–3009.
- [21] S. Kim, H. Park, *RSC Adv.* 3 (2013) 17551–17558.
- [22] M. Liberatore, L. Burtone, T.M. Brown, A. Reale, A. Di Carlo, F. Decker, S. Caramori, C.A. Bignozzi, *Appl. Phys. Lett.* 94 (2009) 173113.
- [23] C.Y. Hu, K. Chu, Y.H. Zhao, W.Y. Teoh, *ACS Appl. Mater. Interfaces* 6 (2014) 18558–18568.
- [24] I. Barcelo, E. Guillen, T. Lana-Villarreal, R. Gomez, *J. Phys. Chem. C* 117 (2013) 22509–22517.
- [25] Z.F. Bian, T. Tachikawa, S.C. Cui, M. Fujitsuka, T. Majima, *Chem. Sci.* 3 (2012) 370–379.
- [26] P. Jayabal, S. Gayathri, V. Sasirekha, J. Mayandi, V. Ramakrishnan, *J. Photochem. Photobiol. A: Chem.* 305 (2015) 37–44.
- [27] J. Peng, Q.J. Sun, Z.C. Zhai, J.Y. Yuan, X.D. Huang, Z.M. Jin, K.Y. Li, S.D. Wang, H.Q. Wang, W.L. Ma, *Nanotechnology* 24 (2013) 484010.
- [28] S. Loheeswaran, K. Balashangar, J. Jevirshan, P. Ravirajan, *J. Nanoelectron. Optoelectron.* 8 (2013) 484–488.
- [29] W. Kim, T. Tachikawa, T. Majima, W. Choi, *J. Phys. Chem. C* 113 (2009) 10603–10609.
- [30] Y. Park, K.J. McDonald, K.S. Choi, *Chem. Soc. Rev.* 42 (2013) 2321–2337.
- [31] J.Y. Zhang, W.J. Luo, W. Li, X. Zhao, G.G. Xue, T. Yu, C.F. Hang, M. Xiao, Z.S. Li, Z.G. Zou, *Electrochim. Commun.* 22 (2012) 49–52.
- [32] W.S. dos Santos, L.D. Almeida, A.S. Afonso, M. Rodriguez, J.P. Mesquita, D.S. Monteiro, L.C.A. Oliveira, J.D. Fabris, M.C. Pereira, *Appl. Catal. B: Environ.* 182 (2016) 247–256.
- [33] S. Eda, M. Fujishima, H. Tada, *Appl. Catal. B: Environ.* 125 (2012) 288–293.
- [34] Y.B. Wan, S.H. Wang, W.H. Luo, L.H. Zhao, *Int. J. Photoenergy* (2012) 392865.
- [35] L.H. Mascaro, A. Pockett, J.M. Mitchels, L.M. Peter, P.J. Cameron, V. Celorio, D.J. Fermin, J.S. Sagu, K.G.U. Wijayantha, G. Kociok-Kohn, F. Marken, *J. Solid State Electrochem.* 19 (2015) 31–35.
- [36] M.F. Gromboni, M.A. Araujo, E. Downey, F. Marken, L.H. Mascaro, *J. Solid State Electrochem.* 20 (2016) 273–283.
- [37] H.W. Jeong, T.H. Jeon, J.S. Jang, W. Choi, H. Park, *J. Phys. Chem. C* 117 (2013) 9104–9112.
- [38] W.J. Jo, J.W. Jang, K.J. Kong, H.J. Kang, J.Y. Kim, H. Jun, K.P.S. Parmar, J.S. Lee, *Angew. Chem. Int. Ed.* 51 (2012) 3147–3151.
- [39] P. Kwolek, K. Pilarczyk, T. Tokarski, K. Lewandowska, K. Szacilowski, *Nanoscale* 6 (2014) 2244–2254.
- [40] H. Ye, H.S. Park, A.J. Bard, *J. Phys. Chem. C* 115 (2011) 12464–12470.
- [41] K. Zhang, X.J. Shi, J.K. Kim, J.H. Park, *Phys. Chem. Chem. Phys.* 14 (2012) 11119–11124.
- [42] T.H. Jeon, W. Choi, H. Park, *Phys. Chem. Chem. Phys.* 13 (2011) 21392–21401.
- [43] S.K. Choi, W. Choi, H. Park, *Phys. Chem. Chem. Phys.* 15 (2013) 6499–6507.
- [44] D. Eisenberg, H.S. Ahn, A.J. Bard, *J. Am. Chem. Soc.* 136 (2014) 14011–14014.
- [45] M.Z. Xie, X.D. Fu, L.Q. Jing, P. Luan, Y.J. Feng, H.G. Fu, *Adv. Energy Mater.* 4 (2014) 1300995.
- [46] S. Ho-Kimura, S.J.A. Moniz, A.D. Handoko, J.W. Tang, *J. Mater. Chem. A* 2 (2014) 3948–3953.
- [47] H.W. Jeong, T.H. Jeon, J.S. Jang, W. Choi, H. Park, *J. Phys. Chem. C* 117 (2013) 9104–9112.
- [48] M. Zhou, J. Bao, Y. Xu, J.J. Zhang, J.F. Xie, M.L. Guan, C.L. Wang, L.Y. Wen, Y. Lei, Y. Xie, *ACS Nano* 8 (2014) 7088–7098.
- [49] S. Sodergren, A. Hagfeldt, J. Olsson, S.E. Lindquist, *J. Phys. Chem.* 98 (1994) 5552–5556.
- [50] B.C. O'Regan, S. Scully, A.C. Mayer, E. Palomares, J. Durrant, *J. Phys. Chem. B* 109 (2005) 4616–4623.
- [51] X.T. Zhang, I. Sutanto, T. Taguchi, Q.B. Meng, T.N. Rao, A. Fujishima, H. Watanabe, T. Nakamori, M. Uragami, *Solar energy mater. Solar Cells* 80 (2003) 315–326.
- [52] H. Rensmo, H. Lindstrom, S. Sodergren, A.K. Willstedt, A. Solbrand, A. Hagfeldt, S.E. Lindquist, *J. Electrochem. Soc.* 143 (1996) 3173–3178.
- [53] C.M. Suarez, S. Hernandez, N. Russo, *Appl. Catal. A: Gen.* 504 (2015) 158–170.
- [54] A.F. Palmstrom, P.K. Santra, S.F. Bent, *Nanoscale* 7 (2015) 12266–12283.